

# Influence of supramolecular bonding contacts on the spin crossover behaviour of iron(II) complexes from 2,2'-dipyridylamino/*s*-triazine ligandst

Cite this: *Dalton Trans.*, 2013, **42**, 7120Nanthawat Wannarit,<sup>a,c</sup> Olivier Roubeau,<sup>\*b</sup> Sujittra Youngme,<sup>\*c</sup> Simon J. Teat<sup>d</sup> and Patrick Gamez<sup>\*a,e</sup>

Reactions of the related ligands 2-(*N,N*-bis(2-pyridyl)amino)-4,6-bis(phenoxy)-(1,3,5)triazine (**L1**) and 2-(*N,N*-bis(2-pyridyl)amino)-4,6-bis(pentafluorophenoxy)-(1,3,5)triazine (**L1<sup>F</sup>**) with iron(II) thiocyanate produced two spin-crossover coordination compounds with distinct cooperative behaviours. *trans*-[Fe(**L1**)<sub>2</sub>(NCS)<sub>2</sub>]-2CH<sub>2</sub>Cl<sub>2</sub> (**1**) displays a very gradual transition centred at  $T_{\frac{1}{2}} = 233$  K, characterized by a  $\Delta T_{80}$  (namely the temperature range within which 80% of the transition considered occurs) of 90 K, while that of fluorinated *trans*-[Fe(**L1<sup>F</sup>**)<sub>2</sub>(NCS)<sub>2</sub>]-2CH<sub>3</sub>CN (**3**) is significantly more abrupt (and centred at  $T_{\frac{1}{2}} = 238$  K), with a  $\Delta T_{80}$  of 50 K, resulting from supramolecular contacts induced by the fluorinated phenol groups. The coordination compound equivalent to **1** with selenocyanate anions, namely *trans*-[Fe(**L1**)<sub>2</sub>(NCSe)<sub>2</sub>]-4CH<sub>2</sub>Cl<sub>2</sub>-4CH<sub>3</sub>OH (**2**), also exhibits SCO properties centred at  $T_{\frac{1}{2}} = 238$  K, but the transition is very gradual ( $\Delta T_{80} = 150$  K). Light-induced excited spin-state trapping (LIESST) is effective although incomplete for **2** and **3**, while it is complete with a  $T_{\text{LIESST}}$  of 58 K for **1**.

Received 31st January 2013,  
Accepted 27th February 2013

DOI: 10.1039/c3dt50326g

www.rsc.org/dalton

## Introduction

The spin-crossover (SCO) phenomenon is a particularly interesting manifestation of the ligand-field theory.<sup>1,2</sup> Hence, for octahedral d<sup>4</sup>–d<sup>7</sup> transition-metal complexes that may be either low spin (LS) or high spin (HS), the occurrence of SCO is associated with intermediate ligand-field strength,<sup>3</sup> for which the transition-metal compound may present HS ↔ LS bistability through the application of an external stimulus like

temperature, pressure or light.<sup>4–7</sup> Such behaviour is obviously very attractive, especially with d<sup>6</sup> Fe(II) ions for which the LS state is diamagnetic and sharp differences in optical properties are often associated with the SCO; therefore, SCO compounds may find applications in molecular switches,<sup>8</sup> data-storage devices<sup>9,10</sup> and optical displays.<sup>11–13</sup> Consequently, SCO has attracted a great deal of attention from the scientific community during decades, and this area of research has been experiencing a tremendous development since the past 5 years.<sup>14–20</sup> Thus, many SCO iron(II) complexes have been reported, typically exhibiting an octahedral [FeN<sub>6</sub>] core obtained from ligands containing aromatic nitrogen-donor groups, such as pyridine or azole rings.<sup>21–24</sup>

Since 2006, we have been involved in the design and preparation of various types of pyridine-containing ligands for the generation of SCO compounds.<sup>25–29</sup> In particular, one of the families of ligands developed is based on the 1,3,5-triazine (or *s*-triazine) ring.<sup>30</sup> For instance, the ligand 2,4,6-tris(dipyridin-2-ylamino)-1,3,5-triazine (dpytriaz),<sup>31</sup> including three 2,2'-dipyridylamine units on a *s*-triazine ring, has allowed us to synthesize iron(II) coordination compounds with interesting SCO properties.<sup>25,30,32,33</sup> Then, Murray and co-workers have described various dipyridylamino-substituted-triazine ligands, which have produced a number of SCO compounds with distinct transition behaviours,<sup>34–38</sup> thus illustrating the potential of this category of ligands to create molecular switches.

<sup>a</sup>Departament de Química Inorgànica, QBI, Universitat de Barcelona, Martí i Franquès 1-11, 08028, Barcelona, Spain. E-mail: patrick.gamez@qi.ub.es; http://www.bio-inorganic-chemistry-icrea-ub.com; Fax: +34 934907725

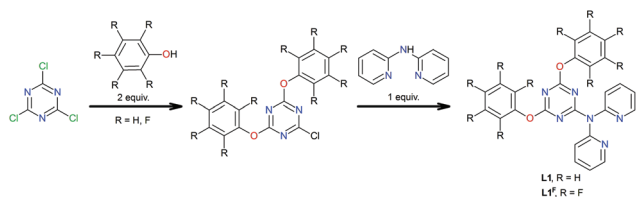
<sup>b</sup>Instituto de Ciencia de Materiales de Aragón (ICMA), CSIC and Universidad de Zaragoza, Plaza San Francisco s/n, 50009 Zaragoza, Spain

<sup>c</sup>Materials Chemistry Research Unit, Department of Chemistry and Centre of Excellence for Innovation in Chemistry, Faculty of Science, Khon Kaen University, Khon Kaen 40002, Thailand

<sup>d</sup>Advanced Light Source, Lawrence Berkeley National Laboratory, 1 Cyclotron Road, Berkeley, CA 94720, USA

<sup>e</sup>Institució Catalana de Recerca i Estudis Avançats (ICREA), Passeig Lluís Companys 23, 08010 Barcelona, Spain

†Electronic supplementary information (ESI) available: Tables S1–S3 summarizing crystallographic and refinement parameters for **1**–**3**; Fig. S1–S4 illustrating particular features of the solid-state structures of **1**–**3**;  $\Delta H$  and  $\Delta S$  for **3** (Fig. S5); a  $d(\chi T)/dT$  vs.  $T$  plot for **3** (Fig. S6); Fig. S7 depicting the single-crystal X-ray structure of **L1**; Table S4 summarizing crystallographic and refinement parameters for **L1**. CCDC 921061–921067 and 922570. For ESI and crystallographic data in CIF or other electronic format see DOI: 10.1039/c3dt50326g



**Scheme 1** Preparation of ligands 2-(*N,N*-bis(2-pyridyl)amino)-4,6-bis(phenoxy)-(1,3,5)triazine (**L1**) and 2-(*N,N*-bis(2-pyridyl)amino)-4,6-bis(pentafluorophenoxy)-(1,3,5)triazine (**L1<sup>F</sup>**).

In the present study, two new members of this family of 2,2'-dipyridylamino/*s*-triazine ligands have been prepared. The straightforward and selective substitutions of the three chloride atoms of 2,4,6-trichloro-1,3,5-triazine by phenolic reagents and 2,2'-dipyridylamine yield the related ligands 2-(*N,N*-bis(2-pyridyl)amino)-4,6-bis(phenoxy)-(1,3,5)triazine (**L1**, R = H; Scheme 1) and 2-(*N,N*-bis(2-pyridyl)amino)-4,6-bis(pentafluorophenoxy)-(1,3,5)triazine (**L1<sup>F</sup>**, R = F; Scheme 1). These two ligands, which differ by the replacement of the hydrogen atoms of the phenoxy groups of **L1** by fluorides (**L1<sup>F</sup>**), have been designed to investigate the role played by supramolecular interactions (*i.e.*  $\pi \cdots \pi$  interactions, halogen bonding) induced by the distinct aryl groups in the SCO properties of the corresponding *trans*-[FeL<sub>2</sub>(NCS)<sub>2</sub>] complexes.

## Results and discussion

### Synthesis and crystal structures

The ligands 2-(*N,N*-bis(2-pyridyl)amino)-4,6-bis(phenoxy)-(1,3,5)triazine (**L1**) and 2-(*N,N*-bis(2-pyridyl)amino)-4,6-bis(pentafluorophenoxy)-(1,3,5)triazine (**L1<sup>F</sup>**) are readily prepared *via* a two-step reaction in THF from 2,4,6-trichloro-1,3,5-triazine, following a straightforward synthetic procedure (Scheme 1 and the Experimental section).<sup>39,40</sup>

Compound **1**, *trans*-[Fe(**L1**)<sub>2</sub>(NCS)<sub>2</sub>] $\cdot$ 2CH<sub>2</sub>Cl<sub>2</sub>, is obtained with a yield of 70% by direct addition of a freshly prepared water/methanol solution of iron(II) thiocyanate (1 equiv.) to a dichloromethane solution containing 2 equiv. of **L1**, which exhibits SCO properties (see section Magnetic studies), crystallizes in the triclinic space group *P* $\bar{1}$ , at 100, 240 and 300 K (Table S1<sup>†</sup>). A representation of the molecular structure of **1** at 100 K (low-spin state) is depicted in Fig. 1. Selected bond lengths and angles are listed in Table 1.

The iron(II) centre in **1** displays the expected octahedral coordination environment, typically observed for iron(II) thiocyanate complexes with this family of dipyridylamino-substituted-triazine ligands.<sup>25,33–38</sup> The metal ion is coordinated by two **L1** ligands in the equatorial plane of the octahedron, the apical positions being occupied by two *trans* thiocyanate anions (Fig. 1). At 100 K, the Fe–N<sub>pyridine</sub> distances in the range 1.981(2)–1.992(2) Å are characteristic of an LS iron(II) ion. The Fe–N<sub>NCS</sub> bond lengths of 1.943(2) Å are also indicative of an LS state. These coordination bond lengths increase by *ca.* 0.22 Å

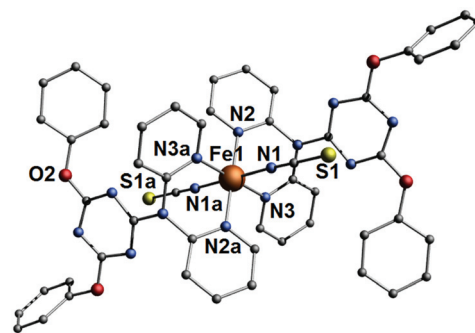


**Fig. 1** Representation of the molecular structure of compound **1** (LS state, determined at 100 K) with a partial atom-numbering scheme. The hydrogen atoms and the lattice dichloromethane molecules are not shown for clarity. Symmetry operation: a, 1 – *x*, 1 – *y*, 1 – *z*.

**Table 1** Coordination bond lengths (Å) and angles (°), and supramolecular interactions for compound **1** at three different temperatures

Bond	100 K (LS)	240 K	300 K (HS)
Fe1–N1	1.943(2)	2.051(2)	2.075(4)
Fe1–N2	1.992(2)	2.163(2)	2.216(3)
Fe1–N3	1.981(2)	2.149(2)	2.203(3)
Fe1 $\cdots$ Fe1 <sub>inter</sub> <sup>a</sup>	10.138(2)	10.239(2)	10.301(4)
Angle <sup>b</sup>	100 K	240 K	300 K
N2–Fe1–N3	86.8(6)	83.5(8)	82.4(1)
N2–Fe1–N3a	93.3(6)	96.5(8)	97.6(1)
N1–Fe1–N1a	180	180	180
$\Sigma$ Fe <sup>c</sup>	31	40	46
$\Phi$ <sup>d</sup>	37	58	67
H-bonding contacts	100 K	240 K	300 K
C11–H11A $\cdots$ O2	3.559(3)	3.609(4)	3.642(8)
C27–H27A $\cdots$ C13	3.415(3)	3.508(4)	3.526(7)
Lone pair $\cdots$ $\pi$ interactions	100 K	240 K	300 K
Cg5 $\cdots$ S1	3.459(1)	3.561(1)	3.598(2)

<sup>a</sup> Closest inter-monomer Fe $\cdots$ Fe distance. <sup>b</sup> Symmetry operation: a, 1 – *x*, 1 – *y*, 1 – *z*. <sup>c</sup>  $\Sigma$  = the sum of  $|90 - \theta|$  for the 12 N–Fe–N angles in the octahedron.<sup>43,44</sup> <sup>d</sup>  $\Phi$  = the sum of  $|60 - \theta|$  for the 24 N–Fe–N angles describing the trigonal twist angle.<sup>15,41</sup>

for Fe–N<sub>pyridine</sub> and *ca.* 0.13 Å for Fe–N<sub>NCS</sub> when the temperature is raised to 300 K (Table 1), which describe a full spin transition that has been observed as well by variable-temperature magnetic susceptibility measurements (see below). At 240 K, the distances found, *i.e.* 2.149(2)–2.163(2) Å for Fe–N<sub>pyridine</sub> and 2.051(2) Å for Fe–N<sub>NCS</sub>, correspond to an HS–LS mixture of about 78/22, in agreement with bulk magnetic studies.

The distortion parameters  $\Sigma$  and  $\Phi$  gauge the magnitude of the deformation of the coordination geometry relative to a perfect octahedron (for which  $\Sigma = \Phi = 0$ ).<sup>15,41,42</sup> For LS **1**,  $\Sigma = 31$  and  $\Phi = 37$  and these values increase to respectively 46 and 67 for the HS state (Table 1).  $\Delta\Sigma$  ( $\Sigma_{\text{HS}} - \Sigma_{\text{LS}}$ ) and  $\Delta\Phi$  ( $\Phi_{\text{HS}} - \Phi_{\text{LS}}$ ) thus illustrate the extent of the structural changes that take place during the spin transition. For **1**,  $\Delta\Sigma = 15$  and  $\Delta\Phi = 30$ . The high  $\Delta\Phi$  value indicates a severe distortion of the

original octahedral geometry towards a trigonal prismatic structure, a feature that is commonly noticed upon LS  $\rightarrow$  HS transition.<sup>15</sup> Such a structural distortion may affect the degree of interaction between the spin active species, resulting in cooperativity between the switching centres that is normally reflected by an abrupt LS  $\leftrightarrow$  HS crossover phenomenon. Actually, the magnetic studies (see below) reveal a weakly cooperative behaviour since a complete HS-to-LS conversion is realized within a temperature range of *ca.* 90 K (see section Magnetic studies).

The crystal packing of **1** shows that the iron(II) centres weakly interact along the crystallographic *c* axis through C–H...O and C–H... $\pi$  contacts (which are affected by the transition; see Table 1), producing a supramolecular 1D chain (Fig. 2A). These chains do not significantly interact with each other (Fig. 2B), which may explain the moderate cooperativity of the SCO behaviour observed by magnetic measurements (see below).

In addition, the molecules of **1** display intramolecular lone pair... $\pi$  interactions<sup>45</sup> between the thiocyanate sulfur atoms and the triazine rings (Cg5...S1 = 3.459(1) Å; Fig. S1†).

Compound **2**, *trans*-[Fe(L1)<sub>2</sub>(NCSe)<sub>2</sub>] $\cdot$ 4CH<sub>2</sub>Cl<sub>2</sub> $\cdot$ 4CH<sub>3</sub>OH, is obtained with a yield of 63%, applying the same synthetic procedure as that used to prepare **1**, replacing iron(II) thiocyanate by iron(II) selenocyanate. As anticipated, **2** is an SCO compound (see section Magnetic studies), which crystallizes in the monoclinic space group *P*<sub>2</sub><sub>1</sub>/*c* in its LS state (Table S2†). A view of the molecular structure of **2** is shown in Fig. 3.

Unsurprisingly, the coordination environment of the iron(II) ion in **2** is similar to that of **1** (see Fig. 1 and 3). The observed octahedral geometry is formed by four pyridine donors in the equatorial plane (belonging to two L1 ligands) and two axial NCSe<sup>−</sup> anions. The Fe–N<sub>pyridine</sub> bond lengths ranging from 1.992(4) to 2.009(4) Å and the Fe–N<sub>NCSe</sub> distances of 1.940(4) Å

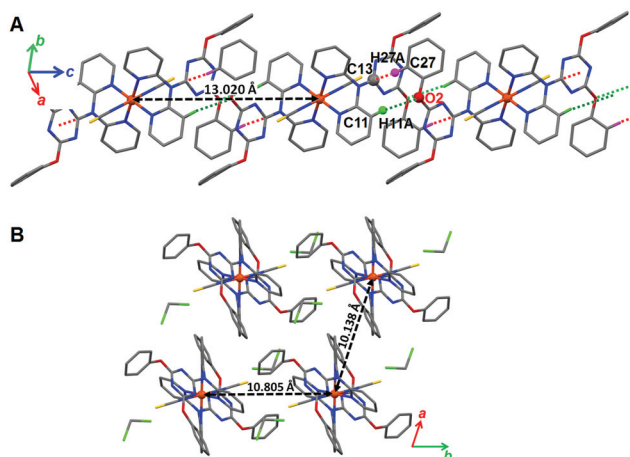


**Fig. 2** Views of the crystal packing of LS **1** showing (A) the formation of a supramolecular 1D chain along the crystallographic *c* axis by means of weak C–H...O and C–H... $\pi$  contacts (respectively C11–H11A...O2 = 3.559(3) Å, green dotted lines and C27–H27A...C13 = 3.415(3) Å, red dotted lines); (B) the arrangement of the chains in the *ab* plane illustrating the lack of significant interactions between them.

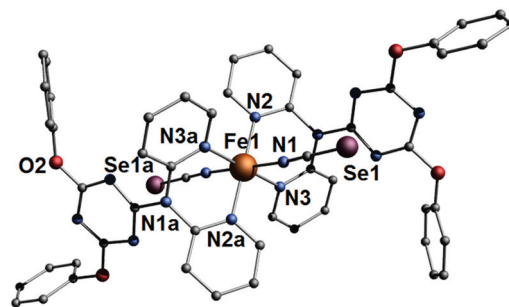


**Fig. 3** Representation of the molecular structure of compound **2** (LS state, determined at 100 K) with a partial atom-numbering scheme. The hydrogen atoms and the lattice dichloromethane molecules are not shown for clarity. Symmetry operation: a, 1 – *x*, 1 – *y*, 1 – *z*.

**Table 2** Coordination bond lengths (Å) and angles (°), and supramolecular interactions for compound **2** (low-spin state)<sup>a</sup>

Bond	100 K (LS)
Fe1–N1	1.940(4)
Fe1–N2	1.992(4)
Fe1–N3	2.009(4)
Fe1...Fe1 <sub>inter</sub> <sup>b</sup>	8.642(4)
Angle	100 K (LS)
N2–Fe1–N3	86.5(2)
N2–Fe1–N3a	93.6(2)
N1–Fe1–N1a	180
$\Sigma$ Fe <sup>c</sup>	25
$\Phi$ <sup>d</sup>	32
$\pi$ ... $\pi$ interactions	100 K (LS)
Cg7...Cg7j	3.717(4)
C22...C24j	3.234(9)
C22...C23j	3.208(8)
C8...C10d	3.796(8)
C–H... $\pi$ contacts	100 K (LS)
C4–H4A...C17g	3.607(7)
C5–H5A...C18g	3.552(7)
Lone pair... $\pi$ interactions	
Cg5...Se1	3.501(2)
Hydrogen bond	
O1s–H1s...O2s	2.828(12)
O1s–H1s...O2s	150(8)
O2s–H2s...N5	3.074(9)
O2s–H2s...N5	155(7)

<sup>a</sup> Symmetry operation: a, 1 – *x*, 1 – *y*, 1 – *z*; d, –*x*, 1 – *y*, 1 – *z*; g, *x*, 1/2 – *y*, 1/2 + *z*; j, –*x*, 1 – *y*, –*z*. <sup>b</sup> Closest inter-monomer Fe...Fe distance. <sup>c</sup>  $\Sigma$  = the sum of  $|90 - \theta|$  for the 12 N–Fe–N angles in the octahedron.<sup>43,44</sup> <sup>d</sup>  $\Phi$  = the sum of  $|60 - \theta|$  for the 24 N–Fe–N angles describing the trigonal twist angle.<sup>15,41</sup>

(Table 2) are typical for an LS iron(II) system, and are comparable to those found for **1** (Tables 1 and 2). Unfortunately, crystallographic data for HS **2** could not be obtained. Actually, single crystals of **2** did not diffract enough at room temperature, most likely as a result of solvent evaporation (and particularly dichloromethane).

The crystal packing of LS **2** reveals the formation of a 1D chain of iron(II) complexes that are connected by parallel-

displaced  $\pi\cdots\pi$  interactions involving the phenyl ring (C21, C22, C23, C24, C25, C26), with a centroid-to-centroid distance of 3.717(4) Å (Cg7...Cg7j; see Table 2 and Fig. 4A). These  $\pi$  stacks are characterized by short C...C contact distances of 3.208(8) Å (C22...C23j) and 3.234(9) Å (C22...C24j). It has to be noted that these  $\pi\cdots\pi$  stacking interactions (which are not occurring in **1**) give rise to a different orientation of the corresponding phenyl rings in compounds **1** and **2** (see phenyl rings of the oxygen atom O2 in Fig. 1 and 3). These chains are weakly interacting with each other *via*  $\pi\cdots\pi$  (C8...C10d) and C-H... $\pi$  (C4-H4A...C17g and C5-H5A...C18g) long contacts (see Table 2 and Fig. 4B).

Surprisingly, although the iron(II) complexes appear to better interact with each other compared to those in **1**, the SCO behaviour of **2** is clearly much less cooperative; actually, the transition is very gradual as the HS state is fully converted into the LS state within a temperature range of over 150 K (see section Magnetic studies). This feature may be explained by the presence of numerous solvent molecules in the crystal lattice of **2**. Indeed, compound **2** is surrounded by 8 solvent molecules, *i.e.* 4CH<sub>3</sub>OH and 4CH<sub>2</sub>Cl<sub>2</sub>, while only 2CH<sub>2</sub>Cl<sub>2</sub> are found for **1**. Therefore, all these solvent molecules in **2** (which are interacting with each other and with the complex; see hydrogen bonds in Table 2) most likely affect the propagation of the spin transition; hence, the behaviour of **2** resembles that of a diluted system (see Fig. S2†), in which the metal centres within the solid are transiting independently, thus resulting in a non-cooperative conversion following Boltzmann population of states.

Finally, similarly to **1**, the molecules of **2** display intramolecular lone pair... $\pi$  interactions between the selenocyanate

selenium atoms and the triazine rings (Cg5...Se1 = 3.501(2) Å; Fig. S3†).

Compound **3**, *trans*-[Fe(L1<sup>F</sup>)<sub>2</sub>(NCS)<sub>2</sub>] $\cdot$ 2CH<sub>3</sub>CN, is prepared with a yield of 65% by direct addition of a freshly prepared water-acetonitrile solution of iron(II) thiocyanate (1 equiv.) to an acetonitrile solution containing 2 equiv. of L1<sup>F</sup>. As the previous two complexes, **3** exhibits spin-transition properties (see section Magnetic studies). **3** crystallizes in the triclinic *P* $\bar{1}$  space group at 100, 190 and 280 K (Table S3†). Selected coordination bond distances and angles are listed in Table 3. A view of the molecular structure of **3** is depicted in Fig. 5.

**Table 3** Coordination bond lengths (Å) and angles (°), and supramolecular interactions for compound **3** at three different temperatures

Bond	100 K (LS)	190 K	280 K (HS)
Fe1-N1	1.937(1)	1.943(1)	2.056(3)
Fe1-N2	1.979(1)	1.985(2)	2.194(2)
Fe1-N3	1.988(1)	1.989(1)	2.207(2)
Fe1...Fe1 <sub>inter</sub> <sup>a</sup>	8.350(1)	8.412(1)	8.643(2)
Angle <sup>b</sup>	100 K	190 K	280 K
N2-Fe1-N3	86.16(5)	86.19(6)	81.83(9)
N2-Fe1-N3a	93.85(5)	93.81(6)	98.17(9)
N1-Fe1-N1a	180	180	180
$\Sigma$ Fe <sup>c</sup>	30	30	41
$\Phi$ <sup>d</sup>	36	36	72
$\pi\cdots\pi$ interactions <sup>b</sup>	100 K	190 K	280 K
O1...C16c	3.112(2)	3.118(3)	3.092(4)
O1...C17c	3.255(2)	3.247(3)	3.238(4)
C15...C16c	3.387(2)	3.378(3)	3.385(5)
Cg3...Cg3b	3.757(1)	3.747(1)	3.787(2)
Halogen...halogen contacts <sup>b</sup>	100 K	190 K	280 K
F8...F9l	2.781(2)	2.803(2)	2.815(4)
Lone pair... $\pi$ interactions	100 K	190 K	280 K
Cg5...S1	3.457(1)	3.489(1)	3.579(2)

<sup>a</sup> Closest inter-monomer Fe...Fe distance. <sup>b</sup> Symmetry operation: a, 1 - x, 1 - y, 1 - z; b, -1 + x, y, z; c, 1 - x, 1 - y, 2 - z; l, 2 - x, 2 - y, 1 - z. <sup>c</sup>  $\Sigma$  = the sum of |90 -  $\theta$ | for the 12 N-Fe-N angles in the octahedron. <sup>d</sup>  $\Phi$  = the sum of |60 -  $\theta$ | for the 24 N-Fe-N angles describing the trigonal twist angle.<sup>15,41</sup>

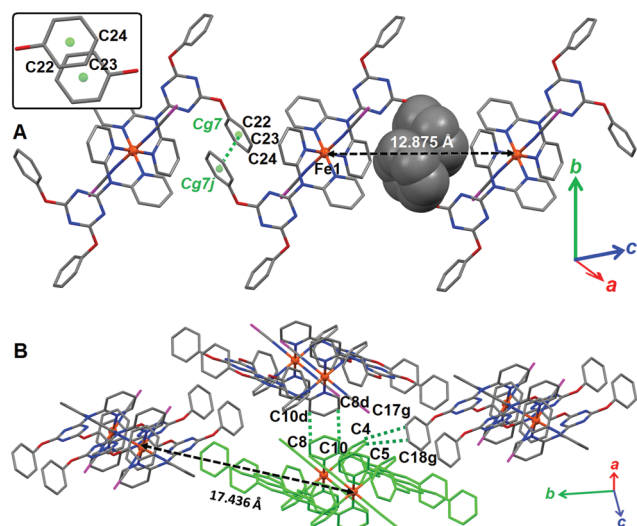


**Fig. 4** Views of the crystal packing of LS **2** showing (A) the formation of a supramolecular 1D chain *via* parallel-displaced  $\pi\cdots\pi$  interactions (Cg7...Cg7j) = 3.717(4) Å (the inset illustrates a parallel-displaced  $\pi\cdots\pi$  stack); (B) the feeble interactions of the chains (one chain is shown in green) by means of weak  $\pi\cdots\pi$  (C8...C10d = 3.796(8) Å) and C-H... $\pi$  (C4-H4A...C17g = 3.607(7) Å and C5-H5A...C18g = 3.552(7) Å) contacts. Symmetry operations: d, -x, 1 - y, 1 - z; g, x, 1/2 - y, 1/2 + z; j, -x, 1 - y, -z.

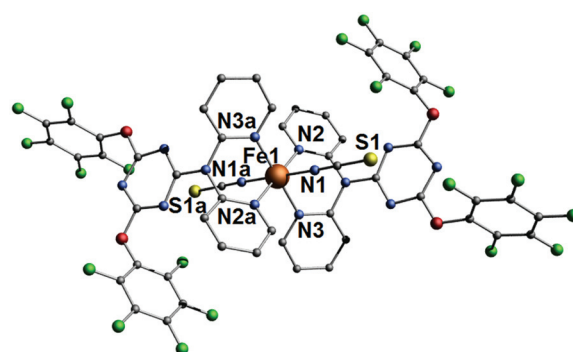


**Fig. 5** Representation of the molecular structure of compound **3** (LS state, determined at 100 K) with a partial atom-numbering scheme. The hydrogen atoms and the lattice acetonitrile molecules are not shown for clarity. Symmetry operation: a, 1 - x, 1 - y, 1 - z.

The coordination environment of the iron(II) ion in **3** is analogous to those of compounds **1** and **2**. The equatorial plane of the octahedron contains four pyridine donors belonging to two  $L1^F$  ligands, and the axial positions are occupied by two thiocyanate anions. At 100 K, the Fe–N<sub>pyridine</sub> and Fe–N<sub>NCS</sub> coordination bond lengths are typical for an LS FeN<sub>6</sub> (Table 3), and are comparable to those of **1** and **2**. For HS **3** at 280 K, these bond distances increase by respectively *ca.* 0.22 and 0.12 Å (Table 3), thus giving characteristic values for this spin state. This full LS → HS transition is corroborated by magnetic measurements (see below). At 190 K, the Fe–N<sub>pyridine</sub> and Fe–N<sub>NCS</sub> distances are indicative of an LS–HS mixture of about 95/5, in agreement with the data obtained by magnetic-susceptibility measurements (see below).

The distortion parameters  $\Sigma$  and  $\Phi$  amount to respectively 30 and 36 for LS **3**, and to 41 and 72 for HS **3**. Hence, the corresponding  $\Delta\Sigma$  and  $\Delta\Phi$  values of respectively 11 and 36 again reflect a strong distortion of the octahedral geometry upon LS → HS transition. As mentioned above, such a distortion is often associated with cooperativity between the transiting centres. In the present case,  $\Delta\Phi = 36$  is higher than that found for the related complex **1** ( $\Delta\Phi = 30$ ). Therefore, a greater cooperative behaviour is expected for **3** in comparison to **1**; in fact, a clearly more abrupt transition (see the corresponding  $\chi T$  vs.  $T$  plots below) is observed for **3**, which may be rationalized by specific crystal-packing features induced (at least in part) by the fluorinated ligand  $L1^F$ .

Actually, the crystal packing of LS **3** reveals an intricate network of strong supramolecular bonds (Fig. 6). First, molecules of **3** are connected *via* strong lone pair... $\pi$  (O1...C16c and O1...C17c; see Table 3 and Fig. 6A) and  $\pi$ ... $\pi$  (C15...C16c; see Table 3 and Fig. 6A) interactions. It has to be noted that the O1...C16c contact distance of 3.112(2) Å is below the sum of the van der Waals radii of O and C (*i.e.* 3.22 Å), thus indicating a very strong interaction between the fluorinated aromatic rings (through lone pair... $\pi$  interactions<sup>46–48</sup>). These supramolecular bonds generate a 1D chain that runs along the crystallographic  $c$  axis. Next, the 1D chains are associated by means of nearly face-to-face  $\pi$ ... $\pi$  interactions between coordinated pyridine moieties characterized by a centroid-to-centroid distance of 3.757(1) Å (see Table 3 and Fig. 6B). This spatial arrangement produces a 2D supramolecular sheet in the  $ac$  plane (Fig. 6B). Finally, the 2D sheets are connected to each other by double strong F...F bonds (indeed, the F8...F9I distance of 2.781(2) Å is well below the sum of the van der Waals radii of two F atoms, namely 2.94 Å),<sup>49</sup> giving rise to a 3D framework (Fig. 6C).

In summary, the transiting iron(II) centres are very well linked to each other (within all the crystal lattice, in contrast to **1** and **2**). Moreover, the solid-state structure of **3** includes less lattice solvent molecules than **2** (which contains 8 molecules of the solvent per iron(II) complex); hence **3** is clearly the most compact of the three systems. Therefore, an efficient cooperative behaviour may be expected for **3**. As a matter of fact, the magnetic studies show the steepest HS ↔ LS transition for **3**, which is completed within a temperature range of

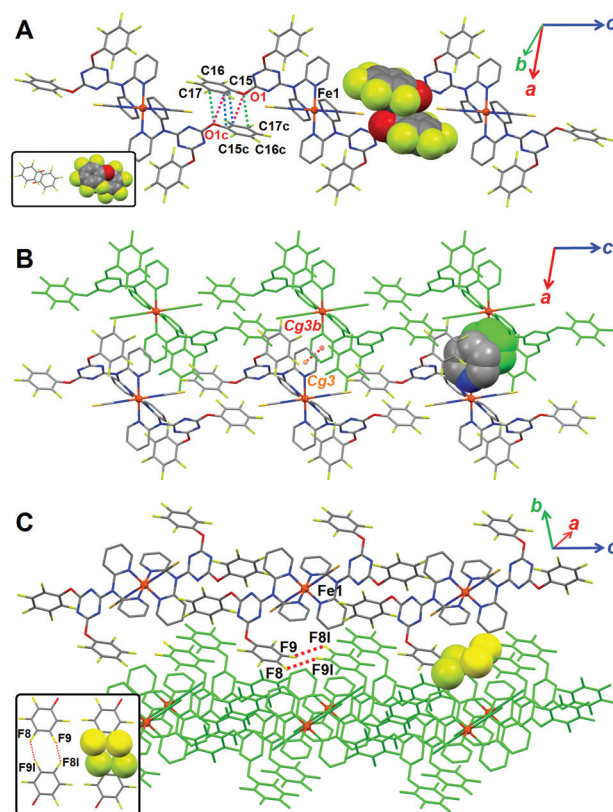


**Fig. 6** Views of the crystal packing of LS **3** showing (A) the formation of a supramolecular 1D chain *via* parallel-displaced pentafluorophenyl...pentafluorophenyl interactions (O1...C16c = 3.112(2) Å, O1...C17c = 3.255(2) Å and C15...C16c = 3.387(2) Å) (the inset illustrates the occurrence of a parallel-displaced stack between two pentafluorophenyl rings); (B) the formation of 2D sheets by means of  $\pi$ ... $\pi$  interactions between coordinated pyridine rings (Cg3...Cg3b = 3.757(1) Å). One supramolecular chain is shown in green; (C) the formation of a 3D supramolecular framework through the connection of the 2D sheets by strong F...F bonding contacts (F8...F9I = 2.781(2) Å) (the inset illustrates the bonding interaction of pentafluorophenyl rings *via* double halogen...halogen contacts), a 2D supramolecular sheet is shown in green. Symmetry operations:  $b, -1 + x, y, z$ ;  $c, 1 - x, 1 - y, 2 - z$ ;  $l, 2 - x, 2 - y, 1 - z$ .

*ca.* 50 K (while it is about 90 K for **1** and 150 K for **2**; see below).

As for **1** and **2**, lone pair... $\pi$  interactions are realized between the thiocyanate sulfur atoms and the triazine rings (Cg5...S1 = 3.457(1) Å; Fig. S4†).

### Magnetic, photomagnetic and thermal studies

Confirmation of the process of thermal SCO indicated by the structural observations on single crystals of **1–3** was obtained through magnetization measurements on bulk samples in the temperature range 5–300 K. The resulting temperature dependencies of the  $\chi T$  product (Fig. 7),  $\chi$  being the molar paramagnetic susceptibility, evidence for all three compounds a complete and gradual thermal SCO. For compound **1**, the  $\chi T$  product is 3.19 cm<sup>3</sup> mol<sup>-1</sup> K at 300 K, a value typical for an Fe(II) ion in an HS  $S = 2$  state.  $\chi T$  starts to decrease already from 300 K to reach values of *ca.* 0.11–0.07 cm<sup>3</sup> mol<sup>-1</sup> K below 160, which are now indicative of a fully populated LS  $S = 0$

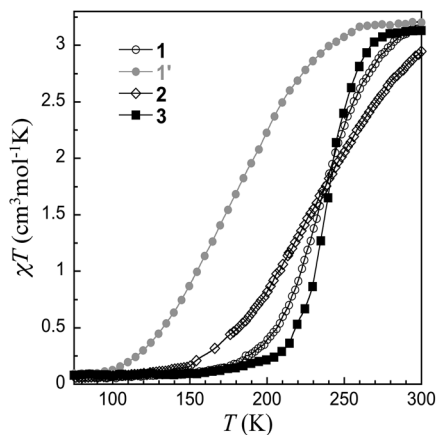


**Fig. 7**  $\chi T$  vs.  $T$  plot for **1** (empty circles), **1'** (full circles), **2** (empty rhomboids) and **3** (full squares) showing the complete and gradual SCO. Lines are only guides to the eye.

state. The corresponding transition is centred at  $T_{\frac{1}{2}} = 233$  K. The selenocyanate derivative **2** exhibits a more gradual SCO centred at  $T_{\frac{1}{2}} = 228$  K, with a  $\chi T$  value of only  $2.95 \text{ cm}^3 \text{ mol}^{-1} \text{ K}$  at 300 K (thus suggesting that the transition process has already started to take place at this temperature), and  $<0.10 \text{ cm}^3 \text{ mol}^{-1} \text{ K}$  below 130 K. In contrast, the SCO process, centred at  $T_{\frac{1}{2}} = 238$  K, is more abrupt for **3** (as a result of a better cooperativity; see above), with a decrease of  $\chi T$  from  $3.10 \text{ cm}^3 \text{ mol}^{-1} \text{ K}$  at 280 K down to  $0.2\text{--}0.1$  below 200 K. This comparatively more cooperative character is illustrated by a smaller  $\Delta T_{80}$  value of 50 K (80% of the transition occurs within about 50 K) for **3**, compared to those observed for **1** and **2**, respectively, at 90 and 150 K. These observations are reproduced upon warming, thus without detectable hysteresis, and over various cycles and batches, although only for fresh crystalline material in the case of **1**. Indeed, a more gradual, though complete, SCO centred at *ca.* 173 K is detected for the poorly crystalline powder **1'** obtained upon air exposure of **1**, which is ascribed to the loss of lattice solvent molecules (as indicated by Elemental Analysis; see the Experimental section). The observation of a similar  $T_{\frac{1}{2}}$  for the thiocyanate and selenocyanate derivatives **1** and **3** agrees with our previous report with the related complexes obtained with the ligand 6-chloro-*N,N*-di(pyridin-2-yl)-1,3,5-triazine-2,4-diamine.<sup>33</sup> It thus seems that the replacement of S by Se in this family of *trans*-[Fe<sup>II</sup>L<sub>2</sub>(NCX)<sub>2</sub>] compounds has only little influence on the SCO temperature, in contrast to other NCX-based SCO compounds.<sup>50–54</sup>

Confirmation of the relatively cooperative character of the SCO for **3** was obtained from Differential-Scanning Calorimetry (DSC). Indeed, while only very broad poorly energetic humps are detected for **1'** and **2**, the molar heat capacity of **3** at constant pressure,  $C_p$ , exhibits a strong anomaly between 200 and 280 K, culminating at *ca.* 237 K (see Fig. 8), which can be attributed to the SCO phenomenon in **3**. Both the associated excess enthalpy and entropy are relatively large, respectively, at  $11.70 \text{ kJ mol}^{-1}$  and  $49.6 \text{ J mol}^{-1} \text{ K}^{-1}$  (see the Experimental section and Fig. S5†), which is usually seen as a consequence

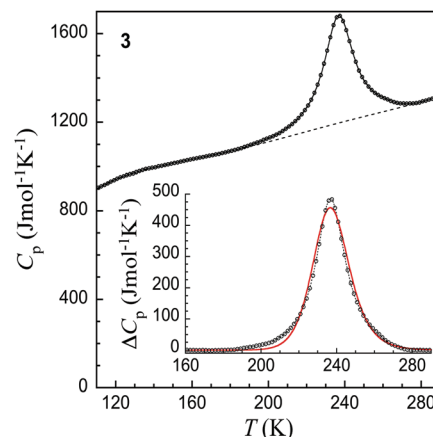


**Fig. 8** Molar heat capacities of **3** showing a broad hump associated with the SCO. The dashed line is the estimated lattice component. Inset: excess heat capacities associated with the SCO in **3**. The full line is a fit to the domain model of Sorai (see the text and ref. 57) with  $n = 6.2$ .

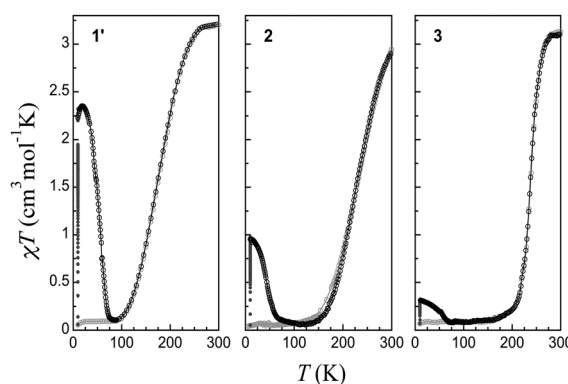


**Fig. 9**  $\chi T$  vs.  $T$  plot for **1'** (left), **2** (middle) and **3** (right), showing the process of SCO (grey empty circles), the (partial) LS to HS photo-induced trapping at 10 K (full circles) and the relaxation back to the LS ground state and normal behaviour upon warming (black empty circles).

of a cooperative character of the SCO.<sup>55,56</sup> In particular, the excess entropy is well above the purely electronic component,  $R \ln 5$ ; it thus encloses a significant content arising from the coupling of the electronic transition with lattice phonons. Fitting the excess heat capacity of **3** to Sorai's domain model<sup>57</sup> results in a number of interacting molecules per domain of  $n = 6.2$  (red line in the inset of Fig. 8), which is characteristic of a relatively cooperative SCO, in agreement with the magnetic studies (Fig. 9).

Preliminary photomagnetic studies on thin samples of **1'**, **2** and **3** indicate that an HS metastable state can be trapped for all three compounds at low temperatures through the so-called LIESST effect,<sup>58</sup> although with distinct efficacies. Indeed, while an increase of  $\chi T$  is detected upon irradiation in the 500–650 nm range at 10 K, the initial rate of increase is highest for **1'**, and smallest for **3**, for a similar sample thickness. In addition, the rate of increase drops more rapidly for **2** and **3**, with stable values, corresponding to incomplete trapping of at most 40 and 20% HS respectively, reached at longer

irradiation times. On the other hand, a full HS state can be trapped in the case of **1'**. Upon warming, an increase of  $\chi T$  is first observed, which corresponds to the Zero-Field Splitting effect of trapped HS species. Subsequently, a decrease gradually sets in, which is due to the thermally-activated relaxation back to the LS state that is reached at *ca.* 85 K. A characteristic  $T_{\text{LIESST}}$  temperature of 58 K can be defined,<sup>59</sup> through the first derivative of  $\chi T$  (Fig. S6†). For the other two compounds,  $\chi T$  decreases already from 10 K to reach values similar to those of the normal LS state at *ca.* 70 K. Thus, even with a partial trapping, relaxation of the trapped HS species back to the LS ground state is not as fast at low temperatures as in the previously reported compound *trans*-[Fe(Cladpat)<sub>2</sub>(NCS)<sub>2</sub>].<sup>33</sup> Therefore, considering that the three samples had a similar thickness, the most likely origin of the lack of efficiency of the LIESST effect in **2** and **3** is an overlap of the <sup>5</sup>T<sub>2</sub> → <sup>5</sup>E (HS) band

with an LS band (possibly <sup>1</sup>A<sub>1</sub> → <sup>3</sup>T<sub>1</sub>), giving rise to competitive LIESST and reverse-LIESST processes.<sup>58,60,61</sup>

### SCO systems based on 2,2'-dipyridylamino-substituted triazine ligands and Fe(NCS)<sub>2</sub>

As mentioned earlier, iron(II) complexes of the type *trans*-[Fe<sup>II</sup>L<sub>2</sub>(NCS)<sub>2</sub>], where **L** is a 2,2'-dipyridylamino-substituted triazine ligand (Scheme 2), usually display SCO properties, and the two new members of this family of compounds, namely **1** and **3**, verify this characteristic. Since the first report of such an SCO system by some of us,<sup>25</sup> we and Murray and co-workers have reported a number of 2,2'-dipyridylamino/triazine-based complexes.<sup>33–35,37,38</sup> Relevant structural features and SCO properties of these coordination compounds are described in Table 4. To date, 14 different *trans*-[Fe<sup>II</sup>L<sub>2</sub>(NCS)<sub>2</sub>] complexes have been obtained from 13 distinct ligands. Out of them, two do not show SCO properties; in fact, the simplest member of this family of ligands, namely when **R**<sup>1</sup> = **R**<sup>2</sup> = Cl, does not generate an iron(II) SCO compound.<sup>33</sup> Surprisingly, the *trans*-[Fe<sup>II</sup>L<sub>2</sub>(NCS)<sub>2</sub>] complex whose ligand **L** contains two diphenylamine substituents is also a non-SCO material. All other compounds exhibit SCO properties (complete or incomplete transitions), with  $T_{\frac{1}{2}}$  values ( $T_{\frac{1}{2}}$  corresponds to the temperature at which half of the transiting iron(II) centres have changed their spin state) ranging from 110 up to 260 K, indicating that the transition can be fine-tuned through selection of the R



**Scheme 2** Representation of the *trans*-[Fe<sup>II</sup>L<sub>2</sub>(NCS)<sub>2</sub>] complexes whose structural and SCO properties are described in Table 4. **R**<sup>1</sup> and **R**<sup>2</sup> symbolize different substituents on the triazine ring (see Table 4).

**Table 4** Structural and SCO properties of crystallographically characterized *trans*-[Fe<sup>II</sup>L<sub>2</sub>(NCS)<sub>2</sub>] compounds with 2,2'-dipyridylamino-substituted triazine ligands **L** (Scheme 2)

<b>R</b> <sup>1</sup>	<b>R</b> <sup>2</sup>	Nuclearity	SCO character	SCO behaviour	Hysteresis	$T_{\frac{1}{2}}$	$\Delta\Sigma$	$\Delta\Phi$	Lattice solvent(s)	Ref.
Chlorine	Chlorine	Monomer	—	No	—	—	—	—	H <sub>2</sub> O	33
Chlorine	Aniline	Monomer	Gradual; $\Delta T_{80}^a = 50$ K	Complete	No	178 K	15	27	No	33
Chlorine	Dipyridylamine	Polymer	Very gradual; $\Delta T_{80} \approx 50$ K	Incomplete (half SCO) <sup>b</sup>	No	~205 K	13/9 <sup>c</sup>	26/0 <sup>c</sup>	CH <sub>3</sub> OH	38
Dipyridylamine	Dipyridylamine	Monomer	Gradual; $\Delta T_{80} = 40$ K	Complete	No	200 K	12	31	No	25
Dipyridylamine	Pyridine-4(1H)one	Polymer	Very gradual; $\Delta T_{80} = 77$ K	Complete	No	175 K	12/13 <sup>c</sup>	22/24 <sup>c</sup>	CH <sub>2</sub> Cl <sub>2</sub>	37
Dipyridylamine	Pyridine-4(1H)one	Polymer	Gradual; $\Delta T_{80} = 55$ K	Complete	No	200 K	12/11 <sup>c</sup>	21/6 <sup>c</sup>	CHCl <sub>3</sub> -CH <sub>3</sub> OH	37
Dipyridylamine	Phenol	Polymer	Gradual; $\Delta T_{80} = 39$ K	Incomplete	No	190 K	8/1 <sup>c</sup>	20/6 <sup>c</sup>	H <sub>2</sub> O-CH <sub>3</sub> OH	37
Dipyridylamine	Hydroquinone	Polymer	Gradual; $\Delta T_{80} = 50$ K	Incomplete	No	260 K	4/3 <sup>c</sup>	9/8 <sup>c</sup>	CH <sub>2</sub> Cl <sub>2</sub>	37
Dipyridylamine	Aza-15-crown-5	Polymer	Very gradual; $\Delta T_{80} = 80$ K	Complete	No	110 K	— <sup>d</sup>	— <sup>d</sup>	CH <sub>3</sub> OH	35
Dibenzylamine	Dibenzylamine	Monomer	Gradual; $\Delta T_{80} = 50$ K	Complete	No	~170 K <sup>e</sup>	13	27	No	34
Diphenylamine	Diphenylamine	Monomer	—	No	—	—	—	—	CH <sub>2</sub> Cl <sub>2</sub>	34
Aza-15-crown-5	Aza-15-crown-5	Monomer	Very gradual; $\Delta T_{80} \approx 80$ K	Complete	No	~240 K	14	31	<i>n</i> -C <sub>3</sub> H <sub>7</sub> OH	35
Phenol	Phenol	Monomer	Very gradual; $\Delta T_{80} = 90$ K	Complete	No	233 K	15	30	CH <sub>2</sub> Cl <sub>2</sub>	This work
Pentafluorophenol	Pentafluorophenol	Monomer	Gradual; $\Delta T_{80} = 50$ K	Complete	No	238 K	11	36	CH <sub>3</sub> CN	This work

<sup>a</sup>  $\Delta T_{80}$  is the temperature range within which 80% of the transition considered occurs. <sup>b</sup> The full LS state is not reached as only half of the iron(II) centres are transiting.<sup>38</sup> <sup>c</sup> The compound exhibits two crystallographically distinct iron(II) centres. <sup>d</sup> Only the X-ray structure of the LS compound has been reported.<sup>35</sup> <sup>e</sup> A different polymorphic form of this compound exhibits a very gradual spin transition ( $\Delta T_{80} \approx 85$  K) centred at 300 K.<sup>34</sup>

groups (and the possibilities are limitless). All compounds display very gradual to gradual spin transitions, the more abrupt one ( $\Delta T_{80} = 39$  K) being obtained when  $R^1 =$  dipyridylamine and  $R^2 =$  phenol. It is actually a 1D polymeric chain<sup>37</sup> wherein the cooperativity between the iron(II) ions appears to be relatively efficient. By comparison, when dipyridylamine is replaced by a phenol, *i.e.* when  $R^1 = R^2 =$  phenol, a significantly more gradual behaviour ( $\Delta T_{80} = 90$  K) is observed for the corresponding monomeric species. No hysteretic behaviours have been observed for all these systems; however, it is assumed that careful design of a 2,2'-dipyridylamino-substituted triazine ligand(s) **L** with well-chosen R substituents will allow us to enhance cooperativity between the iron(II) centres that may favour the occurrence of hysteresis.

It can be noted once again that lattice solvent molecules have a great effect on the SCO properties of a coordination compound. Indeed, for the *trans*-[Fe<sup>II</sup>L<sub>2</sub>(NCS)<sub>2</sub>] complex with  $R^1 =$  dipyridylamine and  $R^2 =$  pyridine-4(1*H*)one, distinct SCO behaviours have been obtained in dichloromethane and in chloroform/methanol. In dichloromethane, the compound exhibits a very gradual transition ( $\Delta T_{80} = 77$  K) centred at  $T_{\frac{1}{2}} = 175$  K, while a more abrupt transition ( $\Delta T_{80} = 55$  K) is observed in CHCl<sub>3</sub>-CH<sub>3</sub>OH, at a higher temperature ( $T_{\frac{1}{2}} = 200$  K). This clearly illustrates the sensitivity of the SCO phenomenon, where not only the coordination sphere of the metal ion is important but also the interactions between the complexes in the solid-state and the involvement of lattice solvent molecules (as observed for instance in the present study with compounds **1** and **1'**).

## Conclusions

In the present study, three new members of the still small (but increasing) family of SCO compounds based on the 2,2'-dipyridylamino/*s*-triazine moiety have been obtained and fully characterized. The investigation carried out clearly shows the importance of supramolecular contacts in the cooperativity of the spin-transition process. Indeed, the triazine ligand containing the fluorinated phenolic groups generates a Fe(II)-NCS complex (*i.e.* **3**) whose SCO is significantly more abrupt ( $\Delta T_{80} = 50$  K) than that of the equivalent coordination compound (*i.e.* **1**) with the ligand bearing simple phenolic substituents ( $\Delta T_{80} = 90$  K). These distinct behaviours are obviously due to the fluoride atoms; actually, the F atoms give a  $\pi$ -acidic character to the phenyl rings, hence favouring the occurrence of strong intermolecular  $\pi \cdots \pi$  interactions (which do not take place in the solid-state structure of compound **1**, which lacks the F atoms). In addition, the F atoms are involved in strong intermolecular halogen $\cdots$ halogen bonding contacts (with F $\cdots$ F contact distances well below the sum of the vdW radii), improving further the cooperative character of the SCO.

The exploration of the physical properties of the iron(II) complexes (with NCS or NCSe anions) obtained from the mixed ligand, namely the 2,2'-dipyridylamino/*s*-triazine ligand containing both phenol and pentafluorophenol groups,

represents the next logical step of investigation. Actually, these studies have been initiated by our group and the outcome will be reported in a future paper.

## Experimental section

### Physical measurements

Infra-red spectra (as KBr pellets) were recorded with a Nicolet 5700 FT-IR spectrometer. Elemental analyses were performed by the Servei de Microanàlisi, Consejo Superior de Investigaciones Científicas (CSIC) of Barcelona. <sup>1</sup>H NMR spectra were recorded at room temperature with a Varian Unity 300 MHz spectrometer; chemical shifts are reported in ppm relative to the residual solvent signal of CDCl<sub>3</sub> ( $\delta = 7.26$  ppm).

Variable-temperature magnetic-susceptibility data were collected on microcrystalline samples of **1–3** with Quantum Design SQUID magnetometers housed at either the SAI Physical Measurements of the University of Zaragoza or the Serveis Científicotècnics of the Universitat de Barcelona. Pascal's constants were used to estimate diamagnetic corrections to the molar paramagnetic susceptibility, and a correction was applied for the sample holder. Warming and cooling rates were of the order of 0.3 K min<sup>-1</sup>. Irradiation experiments were performed using the Quantum Design fibre optics setup (FOSH) on thin pellets (<0.5 mm). The applied field was 1 T throughout the whole study. The light source was a Xenon arc lamp equipped with sets of short-pass and long-pass filters (SPF or LPF). Specifically for the present study, an SPF 650 nm and an LPF at 500 nm were used. Data were corrected for the empty FOSH signal, determined beforehand.

Differential Scanning Calorimetry (DSC) experiments were performed with a Q1000 calorimeter with the LNCS accessory from TA Instruments. The temperature and enthalpy scales were calibrated with a standard sample of indium, using its melting transition (156.6 °C, 3296 J mol<sup>-1</sup>). Measurements were carried out using aluminium pans with a mechanical crimp, with an empty pan as a reference. The zero-heat flow procedure described by TA Instruments was followed to derive heat capacities, using a synthetic sapphire as a reference compound. An overall accuracy of *ca.* 0.2 K for the temperature and up to 5 to 10% for the heat capacity was estimated over the whole temperature range, by comparison with the synthetic sapphire. A lattice heat capacity was estimated from the data below and above the anomaly associated with the SCO process (dashed line in Fig. 8). Excess enthalpy and entropy were derived by integration of the excess heat capacity with respect to *T* and Ln*T*, respectively.

### Materials and syntheses

All reactions were performed under aerobic conditions and all reagents and solvents were used as purchased. TLC was performed on Alugram® SIL G/UV/254 silica gel precoated sheets (Macherey-Nagel, Germany). Purification of the organic ligands was carried out by column chromatography using silica gel SDS 60 ACC (0.035–0.070 mm).

### 2-(*N,N*-Bis(2-pyridyl)amino)-4,6-bis(phenoxy)-(1,3,5)triazine (L1)

The synthesis of ligand **L1** was performed in two straightforward steps.

**Preparation of 2-chloro-4,6-bis(phenoxy)-(1,3,5)triazine.** 5.0 g (27.11 mmol) of 2,4,6-trichloro-(1,3,5)triazine were dissolved in 100 mL of dry THF. Two equivalents (7.01 g, 54.22 mmol) of *N,N*-diisopropylethylamine (DIPEA) were added subsequently under stirring. The resulting yellow solution was cooled down to 0 °C, and two equivalents (5.10 g, 54.22 mmol) of phenol were added portionwise. After completion of the addition, the ice bath was removed and the reaction mixture was stirred for 15 min. The white precipitate obtained (identified as a first crop of the chlorhydrate salt of DIPEA) was removed by filtration. The remaining solid was dissolved in diethyl ether and the undissolved white powder corresponding to a second crop of DIPEA-HCl was separated by filtration. Removal of the solvent under reduced pressure produced pure 2-chloro-4,6-bis(phenoxy)-(1,3,5)triazine as a white powder with a yield of 45% (6.08 g, 12.16 mmol). IR (KBr):  $\nu = 3420(\text{w}), 3058(\text{w}), 1578(\text{m}), 1531(\text{s}), 1485(\text{m}), 1455(\text{m}), 1421(\text{m}), 1383(\text{s}), 1293(\text{s}), 1253(\text{m}), 1193(\text{m}), 1162(\text{w}), 1068(\text{w}), 985(\text{w}), 948(\text{s}), 867(\text{w}), 842(\text{w}), 802(\text{w}), 767(\text{m}), 693(\text{m}), 657(\text{w}), 485(5) \text{ cm}^{-1}$ .

**Preparation of 2-(*N,N*-bis(2-pyridyl)amino)-4,6-bis(phenoxy)-(1,3,5)triazine (L1).** One equivalent (1.10 g, 8.80 mmol) of DIPEA was added to a solution of 2-chloro-4,6-bis(phenoxy)-(1,3,5)triazine in 50 mL of dry THF. Next, one equivalent (1.50 g, 8.80 mmol) of 2-dipyridylamine was added and the reaction mixture was refluxed for two hours. Subsequently, the solution was cooled down to room temperature, and the solvent was evaporated under reduced pressure. The solid obtained was dissolved in diethyl ether and the remaining DIPEA-HCl salt was removed by filtration. The resulting crude compound was purified by column chromatography using the solvent mixture  $\text{CH}_2\text{Cl}_2$ -MeOH (99:1) as an eluent. Pure ligand **L1** ( $R_f = 0.42$ ) was obtained as a white crystalline powder with a yield of 55% (2.86 g, 6.58 mmol). Elemental analyses calculated (found) (%) for  $\text{C}_{25}\text{H}_{18}\text{N}_6\text{O}_2$ : C: 69.11 (69.01), H: 4.18 (4.24), N: 19.34 (19.47).  $^1\text{H}$  NMR (300 MHz,  $\text{CDCl}_3$ , room temp.):  $\delta = 8.38\text{--}8.33$  (m, 2H), 7.62 (ddd,  $J = 8.1, 7.5, 2.0$  Hz, 2H), 7.47 (d,  $J = 8.1$  Hz, 2H), 7.33–7.23 (m, 4H), 7.19–7.05 (m, 8H) ppm. IR (KBr):  $\nu = 3427(\text{w}), 3056(\text{w}), 2974(\text{w}), 2857(\text{w}), 1565(\text{m}), 1488(\text{m}), 1432(\text{m}), 1374(\text{s}), 1303(\text{m}), 1238(\text{m}), 1200(\text{m}), 1080(\text{w}), 995(\text{w}), 807(\text{w}), 770(\text{m}), 690(\text{m}) \text{ cm}^{-1}$ . The molecular structure of **L1** was determined by single-crystal X-ray diffraction. A representation of the crystal structure of **L1** is depicted in Fig. S7.† The corresponding crystallographic and refinement parameters are summarized in Table S4.†

### 2-(*N,N*-Bis(2-pyridyl)amino)-4,6-bis(pentafluorophenoxy)-(1,3,5)triazine (L1<sup>F</sup>)

Ligand **L1<sup>F</sup>** was synthesized in a similar manner using pentafluorophenol instead of phenol.

**Preparation of 2-chloro-4,6-bis(pentafluorophenoxy)-(1,3,5)triazine.** 5.0 g (27.11 mmol) of 2,4,6-trichloro-1,3,5-triazine were dissolved in 100 mL of dry THF. Two equivalents (7.01 g, 54.22 mmol) of DIPEA were then added under stirring. The resulting yellow solution was cooled down to 0 °C and two equivalents (9.98 g, 54.22 mmol) of pentafluorophenol were added portionwise. After 15 minutes, the white crystalline precipitate of DIPEA-HCl was separated by filtration and the filtrate was evaporated under reduced pressure. The consequent solid material was dissolved in diethyl ether and the second crop of insoluble DIPEA-HCl was removed by filtration. After evaporation under reduced pressure, pure 2-chloro-4,6-bis(pentafluorophenoxy)-(1,3,5)triazine was obtained as a white powder with a yield of 45% (5.83 g, 11.22 mmol). IR (KBr):  $\nu = 3431(\text{w}), 2991(\text{w}), 2674(\text{w}), 2465(\text{w}), 1655(\text{m}), 1609(\text{s}), 1577(\text{s}), 1522(\text{br,s}), 1475(\text{s}), 1437(\text{m}), 1372(\text{s}), 1306(\text{s}), 1224(\text{w}), 1169(\text{m}), 1155(\text{m}), 1078(\text{s}), 998(\text{s}), 805(\text{m}), 640(\text{w}) \text{ cm}^{-1}$ .

**Preparation of 2-(*N,N*-bis(2-pyridyl)amino)-4,6-bis(pentafluorophenoxy)-(1,3,5)triazine (L1<sup>F</sup>).** One equivalent of (1.10 g, 8.80 mmol) of DIPEA was added to a solution of 2-chloro-4,6-bis(pentafluorophenoxy)-(1,3,5)triazine (4.20 g, 8.80 mmol) in 50 mL of dry THF. Next, one equivalent (1.50 g, 8.80 mmol) of 2-dipyridylamine was added and the resulting reaction mixture was refluxed for two hours. The solution was then cooled down to room temperature, and the solvent was evaporated under reduced pressure. The remaining solid material was dissolved in diethyl ether and the insoluble white powder, *i.e.* DIPEA-HCl, was removed by filtration. The solvent was evaporated under reduced pressure and the crude compound was purified by column chromatography, using the solvent mixture EtOAc-*n*-hexane (50:50) as an eluent. Pure ligand **L1<sup>F</sup>** ( $R_f = 0.63$ ) was obtained with a yield of 55% (2.96 g, 4.82 mmol). Elemental analyses calculated (found) (%) for  $\text{C}_{25}\text{H}_8\text{F}_{10}\text{N}_6\text{O}_2$ : C: 48.88 (50.16), H: 1.31 (1.10), N: 13.68 (13.64). It has to be noted that higher experimental values for C may be obtained with triazine-based compounds.<sup>40</sup>  $^1\text{H}$  NMR (300 MHz,  $\text{CDCl}_3$ , room temp.):  $\delta = 8.40$  (ddd,  $J = 4.9, 1.9, 0.8$  Hz, 2H), 7.73 (ddd,  $J = 8.0, 7.5, 2.0$  Hz, 2H), 7.47 (dt,  $J = 8.1, 0.9$  Hz, 2H), 7.20 (ddd,  $J = 7.5, 4.9, 1.0$  Hz, 2H) ppm. IR (KBr):  $\nu = 3428(\text{w}), 1596(\text{s}), 1562(\text{s}), 1519(\text{s}), 1417(\text{s}), 1435(\text{m}), 1375(\text{s}), 1309(\text{m}), 1305(\text{m}), 1254(\text{m}), 1234(\text{m}), 1166(\text{m}), 1076(\text{s}), 997(\text{s}), 812(\text{w}), 774(\text{w}), 697(\text{w}), 662(\text{w}) \text{ cm}^{-1}$ .

### *trans*-[Fe(L1)<sub>2</sub>(NCS)<sub>2</sub>] $\cdot$ 2CH<sub>2</sub>Cl<sub>2</sub> (1)

A methanolic solution (5 mL) of KNCS (0.019 g, 0.2 mmol) was added to an aqueous solution (2 mL) of  $\text{FeSO}_4\cdot 7\text{H}_2\text{O}$  (0.028 g, 0.1 mmol). After 15 minutes of stirring, the precipitate of  $\text{K}_2\text{SO}_4$  was removed by filtration. Ascorbic acid (in small quantities) was added to the filtrate to prevent oxidation to iron(III). Subsequently, a solution of **L1** (0.086 g, 0.2 mmol) in dichloromethane was added to the iron(II) solution. The resulting yellow reaction mixture was filtered and the filtrate was left unperturbed for the slow evaporation of the solvent. After three days, small yellow single crystals of **1**, suitable for X-ray diffraction studies, were obtained with a yield of 70% (85 mg, 0.07 mmol, based on iron). Elemental analyses calculated

(found) (%) for  $C_{53}H_{38}FeN_{14}O_4S_2Cl_2$  (**1** -  $CH_2Cl_2$ ): C: 56.54 (55.71), H: 3.40 (3.30), N: 17.42 (17.59). IR (KBr):  $\nu = 3435(w)$ , 2067(m), 1604(m), 1556(m), 1488(m), 1376(s), 1309(m), 1245(m), 1201(m), 1016(w), 809(w), 772(w), 688(w)  $cm^{-1}$ .

#### *trans*-[Fe(L1)<sub>2</sub>(NCSe)<sub>2</sub>] $\cdot$ 4CH<sub>2</sub>Cl<sub>2</sub> $\cdot$ 4MeOH (**2**)

Compound **2** was obtained using the synthetic procedure applied to prepare **1**, but using KNCS (0.029 g, 0.2 mmol) instead of KNCS. Single crystals of **2**, suitable for X-ray diffraction studies, were obtained after three days with a yield of 63% (101 mg, 0.063 mmol, based on iron). Elemental analyses calculated (found) (%) for  $C_{55}H_{46}FeN_{14}O_6Se_2Cl_2$  (**2** -  $4CH_2Cl_2$  -  $4MeOH$  +  $3H_2O$ ): C: 52.54 (52.03), H: 3.56 (3.08), N: 16.50 (17.04). IR (KBr):  $\nu = 3425(w)$ , 3066(w), 2074(s), 1602(m), 1559(m), 1487(m), 1435(m), 1373(s), 1311(m), 1249(m), 1194(m), 1077(w), 1018(w), 906(w), 808(w), 767(w), 687(w)  $cm^{-1}$ .

#### *trans*-[Fe(L1<sup>F</sup>)<sub>2</sub>(NCS)<sub>2</sub>] $\cdot$ 2CH<sub>3</sub>CN (**3**)

Compound **3** was obtained applying the synthetic procedure used to prepare **1**, but the ligand L1<sup>F</sup> (0.122 g, 0.2 mmol) was dissolved in acetonitrile instead of dichloromethane. Single crystals of **3**, suitable for X-ray diffraction studies, were obtained after three days with a yield of 65% (96 mg, 0.063 mmol, based on iron). Elemental analyses calculated (found) (%) for  $C_{56}H_{22}F_{20}FeN_{16}O_4S_2$ : C: 45.36 (46.19), H: 1.50 (1.74), N: 15.11 (15.10). IR (KBr):  $\nu = 3464(w)$ , 2056(s), 1610(m), 1557(w), 1519(s), 1475(m), 1372(s), 1309(m), 1241(m), 1078(m), 1000(m), 806(w), 781(w), 753(w), 642(m)  $cm^{-1}$ .

#### X-ray crystallography

X-ray diffraction data for L1 at 250 K, for **1** at 100, 240 and 300 K and for **3** at 100, 190 and 280 K, were collected with a Bruker APEX II CCD diffractometer on the Advanced Light Source beamline 11.3.1 at Lawrence Berkeley National Laboratory, from a silicon 111 monochromator ( $\lambda = 0.7749$  Å). Data for **2** at 100 K were obtained using Mo K $\alpha$  radiation ( $\lambda = 0.7107$  Å) on a Bruker APEX II QUAZAR diffractometer equipped with a microfocus multilayer monochromator. Data reduction and absorption corrections were performed with SAINT and SADABS.<sup>62</sup> The structure of **2** was solved with SIR97,<sup>63</sup> while those of L1, **1** and **3** were solved with SHELXS.<sup>64</sup> All structures were refined on  $F^2$  using the SHELXTL suite.<sup>64</sup> Crystallographic and refinement parameters are summarized in Tables S1–S4. Selected bond distances and angles are given in Tables 1–3. All details can be found in the supplementary crystallographic data for this paper in cif format with CCDC numbers 921061–921067 (coordination compounds **1**–**3**) and 922570 (ligand L1).

#### Acknowledgements

PG acknowledges ICREA (Institutió Catalana de Recerca i Estudis Avançats) and the Ministerio de Economía y Competitividad of Spain (Project CTQ2011-27929-C02-01). NW thanks

the Royal Golden Jubilee Program (RGJ, Grant no. PHD/0234/2550) and Khon Kaen University for a research grant. SY acknowledges The Thailand Research Fund, the National Research University Project of Thailand, Office of the Higher Education Commission, through the Advanced Functional Materials Cluster of Khon Kaen University and the Center of Excellence for Innovation in Chemistry (PERCH-CIC), Office of the Higher Education Commission, Ministry of Education. The Advanced Light Source is supported by the Director, Office of Science, Office of Basic Energy Sciences of the U. S. Department of Energy under contract no. DE-AC02-05CH11231. OR acknowledges funding from the Ministerio de Economía y Competitividad of Spain (Project MAT2011-24284).

#### Notes and references

- B. N. Figgis and M. A. Hitchman, *Ligand Field Theory and Its Applications*, Wiley-VCH, New York, 2000.
- A. B. Koudriavtsev and W. Linert, *J. Struct. Chem.*, 2010, **51**, 335–365.
- R. Boča, in *A Handbook of Magnetochemical Formulae*, Elsevier, London, 2012, pp. 159–186.
- P. Gütllich, A. Hauser and H. Spiering, *Angew. Chem., Int. Ed. Engl.*, 1994, **33**, 2024–2054.
- P. Gütllich and H. A. Goodwin, *Top. Curr. Chem.*, 2004, **233**, 1–47.
- J. A. Real, A. B. Gaspar and M. C. Muñoz, *Dalton Trans.*, 2005, 2062–2079.
- A. Bousseksou, G. Molnár, J. A. Real and K. Tanaka, *Coord. Chem. Rev.*, 2007, **251**, 1822–1833.
- O. Sato, *Proc. Jpn. Acad. Ser. B-Phys. Biol. Sci.*, 2012, **88**, 213–225.
- M. Ruben, E. Breuning, J. M. Lehn, V. Ksenofontov, F. Renz, P. Gütllich and G. B. M. Vaughan, *Chem.-Eur. J.*, 2003, **9**, 4422–4429.
- A. Bousseksou, G. Molnár, P. Demont and J. Menegotto, *J. Mater. Chem.*, 2003, **13**, 2069–2071.
- P. Gütllich, Y. Garcia and H. A. Goodwin, *Chem. Soc. Rev.*, 2000, **29**, 419–427.
- C. Jay, F. Grolière, O. Kahn and J. Kröber, *Mol. Cryst. Liq. Cryst. Sci. Technol., Sect. A*, 1993, **234**, 255–262.
- O. Kahn and C. J. Martinez, *Science*, 1998, **279**, 44–48.
- A. Bousseksou, G. Molnár, L. Salmon and W. Nicolazzi, *Chem. Soc. Rev.*, 2011, **40**, 3313–3335.
- M. A. Halcrow, *Chem. Soc. Rev.*, 2011, **40**, 4119–4142.
- J. Tao, R. J. Wei, R. B. Huang and L. S. Zheng, *Chem. Soc. Rev.*, 2012, **41**, 703–737.
- D. J. Harding, D. Sertphon, P. Harding, K. S. Murray, B. Moubaraki, J. D. Cashion and H. Adams, *Chem.-Eur. J.*, 2013, **19**, 1082–1090.
- K. Bhar, S. Khan, J. S. Costa, J. Ribas, O. Roubeau, P. Mitra and B. K. Ghosh, *Angew. Chem., Int. Ed.*, 2012, **51**, 2142–2145.
- P. Gamez, J. S. Costa, M. Quesada and G. Aromí, *Dalton Trans.*, 2009, 7845–7853.

- 20 G. A. Craig, J. S. Costa, O. Roubeau, S. J. Teat and G. Aromí, *Chem.–Eur. J.*, 2012, **18**, 11703–11715.
- 21 G. Aromí, L. A. Barrios, O. Roubeau and P. Gamez, *Coord. Chem. Rev.*, 2011, **255**, 485–546.
- 22 J. Olguin and S. Brooker, *Coord. Chem. Rev.*, 2011, **255**, 203–240.
- 23 M. Boča, R. F. Jameson and W. Linert, *Coord. Chem. Rev.*, 2011, **255**, 290–317.
- 24 K. S. Murray, *Eur. J. Inorg. Chem.*, 2008, 3101–3121.
- 25 M. Quesada, M. Monrabal, G. Aromí, V. A. de la Peña-O'Shea, M. Gich, E. Molins, O. Roubeau, S. J. Teat, E. J. MacLean, P. Gamez and J. Reedijk, *J. Mater. Chem.*, 2006, **16**, 2669–2676.
- 26 J. S. Costa, K. Lappalainen, G. de Ruiter, M. Quesada, J. K. Tang, I. Mutikainen, U. Turpeinen, C. M. Grünert, P. Gütlich, H. Z. Lazar, J. F. Létard, P. Gamez and J. Reedijk, *Inorg. Chem.*, 2007, **46**, 4079–4089.
- 27 S. Bonnet, M. A. Siegler, J. S. Costa, G. Molnár, A. Bousseksou, A. L. Spek, P. Gamez and J. Reedijk, *Chem. Commun.*, 2008, 5619–5621.
- 28 J. K. Tang, J. S. Costa, S. Smulders, G. Molnár, A. Bousseksou, S. J. Teat, Y. G. Li, G. A. van Albada, P. Gamez and J. Reedijk, *Inorg. Chem.*, 2009, **48**, 2128–2135.
- 29 S. Bonnet, G. Molnár, J. S. Costa, M. A. Siegler, A. L. Spek, A. Bousseksou, W. T. Fu, P. Gamez and J. Reedijk, *Chem. Mater.*, 2009, **21**, 1123–1136.
- 30 M. Quesada, V. A. de la Peña-O'Shea, G. Aromí, S. Geremia, C. Massera, O. Roubeau, P. Gamez and J. Reedijk, *Adv. Mater.*, 2007, **19**, 1397–1402.
- 31 P. Gamez, P. de Hoog, M. Lutz, W. L. Driessen, A. L. Spek and J. Reedijk, *Polyhedron*, 2003, **22**, 205–210.
- 32 M. Quesada, P. de Hoog, P. Gamez, O. Roubeau, G. Aromí, B. Donnadiu, C. Massera, M. Lutz, A. L. Spek and J. Reedijk, *Eur. J. Inorg. Chem.*, 2006, 1353–1361.
- 33 N. Wannarit, O. Roubeau, S. Youngme and P. Gamez, *Eur. J. Inorg. Chem.*, 2013, 730–737.
- 34 T. M. Ross, B. Moubaraki, S. M. Neville, S. R. Batten and K. S. Murray, *Dalton Trans.*, 2012, **41**, 1512–1523.
- 35 T. M. Ross, B. Moubaraki, S. R. Batten and K. S. Murray, *Dalton Trans.*, 2012, **41**, 2571–2581.
- 36 T. M. Ross, B. Moubaraki, K. S. Wallwork, S. R. Batten and K. S. Murray, *Dalton Trans.*, 2011, **40**, 10147–10155.
- 37 T. M. Ross, B. Moubaraki, D. R. Turner, G. J. Halder, G. Chastanet, S. M. Neville, J. D. Cashion, J. F. Létard, S. R. Batten and K. S. Murray, *Eur. J. Inorg. Chem.*, 2011, 1395–1417.
- 38 S. M. Neville, B. A. Leita, D. A. Offermann, M. B. Duriska, B. Moubaraki, K. W. Chapman, G. J. Halder and K. S. Murray, *Eur. J. Inorg. Chem.*, 2007, 1073–1085.
- 39 R. J. Götz, A. Robertazzi, I. Mutikainen, U. Turpeinen, P. Gamez and J. Reedijk, *Chem. Commun.*, 2008, 3384–3386.
- 40 P. de Hoog, P. Gamez, W. L. Driessen and J. Reedijk, *Tetrahedron Lett.*, 2002, **43**, 6783–6786.
- 41 M. Marchivie, P. Guionneau, J. F. Létard and D. Chasseau, *Acta Crystallogr., Sect. B: Struct. Sci.*, 2005, **61**, 25–28.
- 42 J. K. McCusker, A. L. Rheingold and D. N. Hendrickson, *Inorg. Chem.*, 1996, **35**, 2100–2112.
- 43 M. Quesada, F. Prins, E. Bill, H. Kooijman, P. Gamez, O. Roubeau, A. L. Spek, J. G. Haasnoot and J. Reedijk, *Chem.–Eur. J.*, 2008, **14**, 8486–8499.
- 44 P. Guionneau, M. Marchivie, G. Bravic, J. F. Létard and D. Chasseau, *Top. Curr. Chem.*, 2004, **234**, 97–128.
- 45 T. J. Mooibroek and P. Gamez, *CrystEngComm*, 2012, **14**, 1027–1030.
- 46 A. Das, S. R. Choudhury, C. Estarellas, B. Dey, A. Frontera, J. Hemming, M. Helliwell, P. Gamez and S. Mukhopadhyay, *CrystEngComm*, 2011, **13**, 4519–4527.
- 47 S. R. Choudhury, P. Gamez, A. Robertazzi, C. Y. Chen, H. M. Lee and S. Mukhopadhyay, *Cryst. Growth Des.*, 2008, **8**, 3773–3784.
- 48 T. J. Mooibroek and P. Gamez, *CrystEngComm*, 2012, **14**, 3902–3906.
- 49 T. J. Mooibroek and P. Gamez, *CrystEngComm*, 2013, **15**, 1802–1805.
- 50 M. Sorai and S. Seki, *J. Phys. Chem. Solids*, 1974, **35**, 555–570.
- 51 L. Capes, J. F. Létard and O. Kahn, *Chem.–Eur. J.*, 2000, **6**, 2246–2255.
- 52 T. Buchen, H. Toftlund and P. Gütlich, *Chem.–Eur. J.*, 1996, **2**, 1129–1133.
- 53 J. A. Real, I. Castro, A. Bousseksou, M. Verdaguer, R. Burriel, M. Castro, J. Linares and F. Varret, *Inorg. Chem.*, 1997, **36**, 455–464.
- 54 N. Moliner, M. C. Muñoz, S. Létard, J. F. Létard, X. Solans, R. Burriel, M. Castro, O. Kahn and J. A. Real, *Inorg. Chim. Acta*, 1999, **291**, 279–288.
- 55 M. Sorai, *Top. Curr. Chem.*, 2004, **235**, 153–170.
- 56 O. Roubeau, M. Castro, R. Burriel, J. G. Haasnoot and J. Reedijk, *J. Phys. Chem. B*, 2011, **115**, 3003–3012.
- 57 The phenomenological domain model proposed by Sorai is widely used when accurate calorimetric data are available. It is based on heterophase fluctuations and gives a measure of cooperativity through the number  $n$  of like-spin SCO centers per interacting domain, the larger the domains are, the more cooperative the transition is. See: M. Sorai, *Chem. Rev.*, 1996, **1106**, 1976–1031.
- 58 A. Hauser, *Top. Curr. Chem.*, 2004, **234**, 155–198.
- 59 J. F. Létard, *J. Mater. Chem.*, 2006, **16**, 2550–2559.
- 60 A. Hauser, *Top. Curr. Chem.*, 2004, **233**, 49–58.
- 61 A. Hauser, *J. Chem. Phys.*, 1991, **94**, 2741–2748.
- 62 *SAINT, SADABS and SHELXTL*, Bruker AXS, Inc., Madison, WI, USA, 2002.
- 63 A. Altomare, M. C. Burla, M. Camalli, G. L. Casciarano, C. Giacovazzo, A. Guagliardi, A. G. G. Moliterni, G. Polidori and R. Spagna, *J. Appl. Crystallogr.*, 1999, **32**, 115–119.
- 64 G. M. Sheldrick, *Acta Crystallogr., Sect. A: Fundam. Crystallogr.*, 2008, **64**, 112–122.